

# AN INTERACTIVE METHOD OF ANATOMICAL SEGMENTATION AND GENE EXPRESSION ESTIMATION FOR AN EXPERIMENTAL MOUSE BRAIN SLICE

Anton Osokin<sup>(1)</sup>, Dmitry Vetrov<sup>(1)</sup>, Alexey Lebedev<sup>(1)</sup>, Vladimir Galatenko<sup>(1)</sup>, Dmitry Kropotov<sup>(2)</sup>, Konstantin Anokhin<sup>(3)</sup>

(1) Moscow State University

Russia, 119991, Moscow, Vorobyevy gory, 1, anton.osokin@gmail.com, VetrovD@yandex.ru

(2) Dorodnicyn Computing Centre of Russian Academy of Sciences

Russia, 119333, Moscow, Vavilova str., 40, dmitry.kropotov@gmail.com

(3) P.K. Anokhin Institute of Normal Physiology

Russia, 103008, Moscow, Bolshaya Nikitskaya, 6, bld. 4, k\_anokhin@yahoo.com

*Keywords:* mouse brain studies, gene expression detection, image segmentation, morphing, Allen Brain Atlas.

**Abstract.** We consider the problem of statistical analysis of gene expression in a mouse brain during cognitive processes. In particular we focus on the problems of anatomical segmentation of a histological brain slice and estimation of slice's gene expression level. The first problem is solved by interactive registration of an experimental brain slice into 3D brain model constructed using Allen Brain Atlas. The second problem is solved by special image filtering and further smart resolution reduction. We also describe the procedure of non-linear correction of atlas slices which improves the quality of the 3D-model significantly.

## 1 Introduction

The analysis of gene expression in a brain is extremely important for cognitive research. Many cognitive functions (e.g. memory consolidation) are regulated by specific genes whose expression starts during some intellectual activity, e.g. training. On the other hand it is known that changes in activity in specific anatomical brain zones reflect the cognitive processes. The combination of anatomical brain map with gene expression patterns and its further statistical processing would allow researchers to discover new genes that are responsible for cognitive processes and new anatomical structures where the functional activity takes place.

Up to the current moment gene expression in animal brains is measured using the following technique. A brain is extracted, frozen and then cut into slices. Each slice is double-stained by Nissl method to highlight histology (see Fig. 1a) and by ISH<sup>1</sup> method which reveals the neurons with expression of corresponding genes (see Fig. 2)<sup>2</sup>. The main problem is to determine brain structures where active genes are located. This problem is difficult even for human experts especially when the slices are obtained using a non-standard section-plane. However there are several atlases for various animals which contain both histological images and the corresponding images where all brain structures are marked by experts [1]. Here we use Allen Mouse Brain Atlas (ABA) [7], which contains a set of 2D coronal mouse brain slices (see Fig. 1b).

---

<sup>1</sup>In Situ Hybridization

<sup>2</sup>In practice it is usually difficult to make a double-stain of one slice and hence the neighboring slices are stained by different methods.

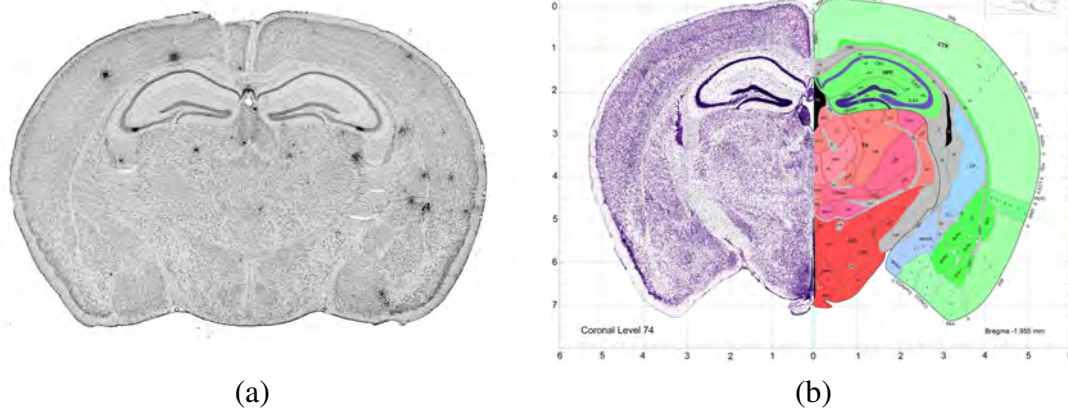


Figure 1: An example of an experimental slice in Nissl stain (a) and an example of brain slice from Allen Brain Atlas with both histological and anatomical views (b).

In the paper we address the problem of semi-automatic segmentation of a brain slice (given by Nissl image, ISH image, or both) into anatomical structures. For this reason we propose the following procedure. First a 3D-model of a mouse brain is constructed using 2D ABA slices. Hence this model contains both histological and anatomical views. Then for the experimental slice we obtain the most similar slice from the constructed 3D model (hereinafter we denote it as a virtual slice) manually by means of special software BrainTravel. At last we transfer the anatomic segmentation of the virtual slice to the experimental slice using a non-linear transformation. For the 3D model we update our previous result [5] by adding a non-linear correction of atlas slices (section 2.1). This correction improves the quality of the 3D model significantly. The virtual slice search process is described in section 2.2 while anatomical segmentation of an experimental slice is given in section 2.3.

In the paper we also consider the problem of numerical estimation of expression level for ISH slices. This is done by a series of filters and detailed in section 3. Finally the paper finishes with a discussion of further work in the area of statistical analysis of gene expression in the brain during cognitive activity.

## 2 Anatomical Segmentation

The procedure of anatomical segmentation of an experimental brain slice consists of several steps. First we register a 2D experimental slice into the 3D-model of mouse brain with information about anatomical structures. During the registration we obtain a virtual slice from the 3D-model that is similar to the experimental one. The virtual slice can be seen in both histological and anatomical modes. Afterwards we find a non-linear deformation of the virtual slice by putting pairs of corresponding keypoints on the histological virtual slice and the experimental slice. Finally we apply the non-linear deformation to the anatomical virtual slice.

### 2.1 Non-Linear Correction of Atlas Slices

As a 3D-model of a mouse brain we use the one from [5]. It was constructed from the set of images from Allen Brain Atlas (ABA). Those images contain information about histology (Nissl stain) and anatomy and are available on-line.<sup>3</sup> At first the slices were aligned linearly, afterwards pairwise deformations were found between all the neighboring slices using cubic B-splines. Finally these deformations were used to fill in the gaps between the atlas slices using morphing transform. The details of the algorithm are given in [5]. Here we have modified the algorithm by adding one more step – a non-

<sup>3</sup><http://mouse.brain-map.org/atlas/ARA/Coronal/browser.html>

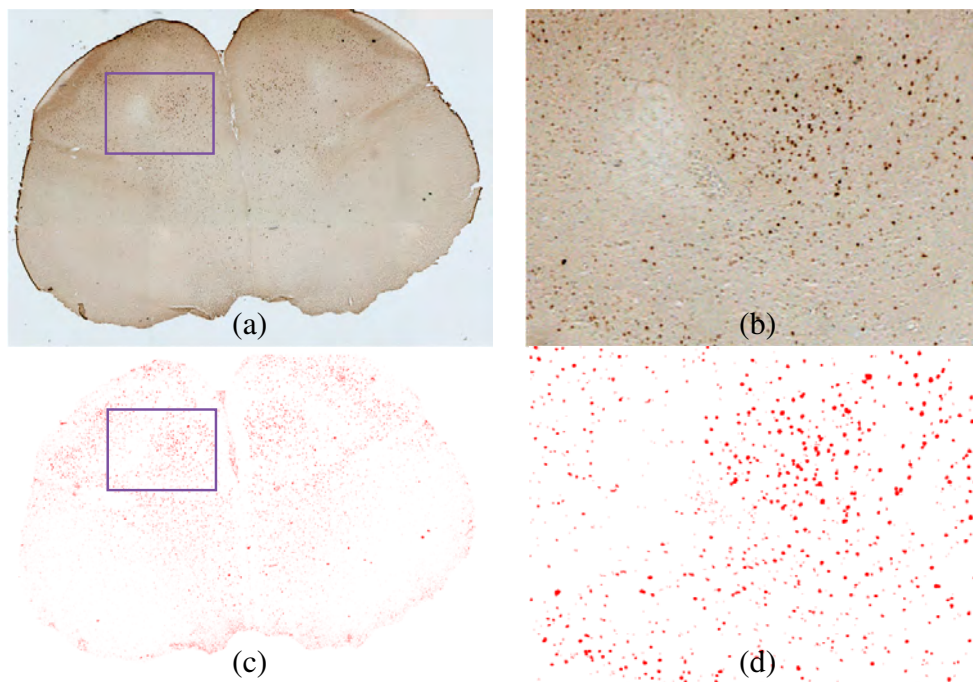


Figure 2: An example of an experimental slice with gene expression in ISH stain. (a) — initial experimental slice; (b) — enlarged part of slice (a); (c) — processed slice (a) using the method from section 3; (d) — enlarged part of image (c).

linear correction of atlas slices. This step is necessary because all the slices from the atlas are independently distorted due to the peculiarities of technological process of their cutting and staining. The application of morphing to uncorrected atlas slices leads to non-smooth histological and anatomical structures which are clearly seen in sagittal projection (see fig. 3a-c). To overcome this problem we used the following approach.

Consider the  $k^{\text{th}}$  uncorrected slice of the atlas  $f_k : \mathbb{R} \times \mathbb{R} \rightarrow \mathbb{R}$ . Our goal is to obtain a corrected slice  $F_k$  that is harmonized with its neighbors. First we compute non-linear deformations  $g_{k,i}$  between it and its  $d$  previous and  $d$  following slices so that

$$f_k \circ g_{k,i} \approx f_i, \quad \forall i = k - d, \dots, k + d.$$

The distance between neighboring slices in ABA is  $100 \mu\text{m}$ , and so the slices lying at the distance of several hundred microns may differ significantly and direct deformation between them may appear inadequate. In the paper we follow [9] and establish the recurrent scheme

$$g_{k,i} = \begin{cases} g_{k,i+1} \circ g_{i+1,i}, & k - d \leq i < k; \\ g_{k,k}, & i = k; \\ g_{k,i-1} \circ g_{i-1,i}, & k < i \leq k + d. \end{cases} \quad (1)$$

The non-linear correction of atlas slices is performed by application of weighted deformation to each slice

$$F_k = f_k \circ \sum_{i=k-d}^{k+d} \gamma_i g_{k,i},$$

where  $\gamma_i = \frac{C_{2d}^{i-k+d}}{2^{2d}}$ . Such non-linear correction of atlas slices before morphing transform yields a much better spatial interpolation (see fig. 3,d-f).

## 2.2 Registration of an Experimental Slice into the 3D Model of Mouse Brain

Suppose we have only ISH experimental slice. Evidently it is impossible to find the correspondent virtual slice in the 3D model automatically, since Nissl and ISH stains differ significantly. Note that Nissl stained slices obtained by different research groups

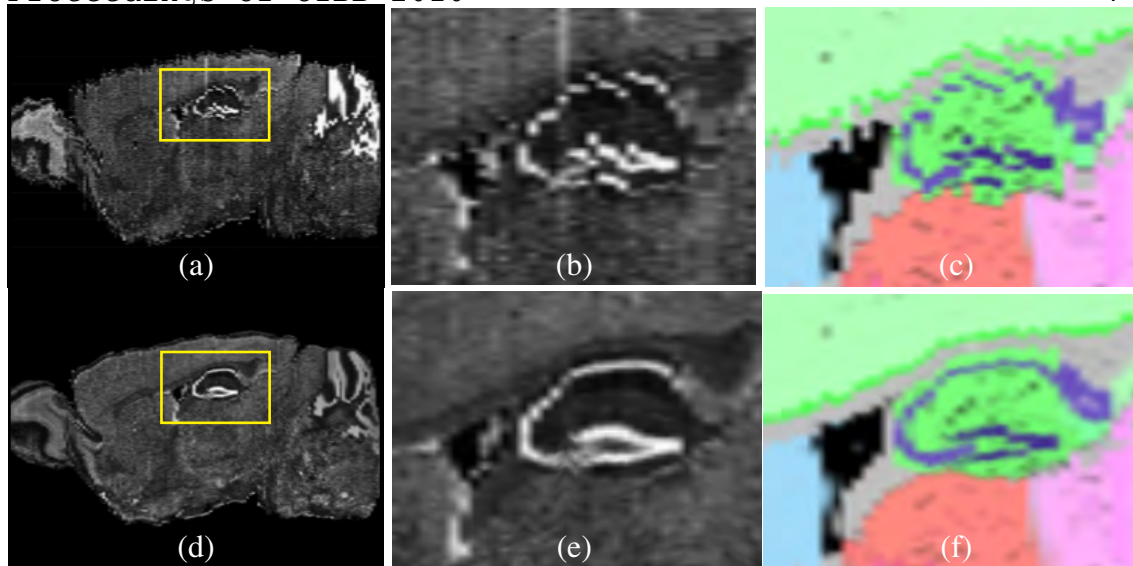


Figure 3: Comparison of different 3D brain models, constructed from 2D ABA slices. (a)-(c) – standard 3D model (simple concatenation of all slices with morphing); (d)-(f) – 3D model, constructed by method from [5] plus the non-linear correction of atlas slices.

could also differ significantly (e.g. in our case Nissl experimental slice differs from Nissl ABA slice). Therefore we developed a special software BrainTravel which allows to navigate through the 3D model and find the correspondent virtual slice manually. We did not expect any difficulties with manual registration of experimental slices using BrainTravel. It usually took us about 2-3 minutes per slice. Note that after registration is finished the virtual and experimental slices are not identical due to the variability of individual brains. Direct transfer of anatomical segmentation to the experimental slice is hence unsuitable (see. fig. 4).

### 2.3 Deformation of Virtual Slice with the aid of Keypoints

In order to obtain a valid anatomical segmentation of the experimental slice we have to deform the virtual slice which was found during the registration process. The difference in stains makes it impossible to apply any method which minimizes the pixel-wise difference between the two images. A possible way out could be the use of information-based methods [4] which are capable to match images of different modalities. In the paper we focused on an alternative approach which seems to be more reliable and is based on the keypoints location. The user assigns keypoints to the corresponding positions in both images. Let  $\{(x_k^1, y_k^1)\}_{k=1}^K$  and  $\{(x_k^2, y_k^2)\}_{k=1}^K$  be the sets of keypoints on the experimental and virtual slices respectively (see fig. 4a,c). We are looking for the deformation  $g : \mathbb{R}^2 \rightarrow \mathbb{R}^2$  of the virtual slice such that it minimizes the following criterion

$$E(g) = \sum_{k=1}^K d((x_k^1, y_k^1), g(x_k^2, y_k^2)) \rightarrow \min_{g(\cdot, \cdot) \in \mathcal{G}},$$

where  $d((x_1, y_1), (x_2, y_2))$  stands for Euclidean distance between the two points. As before we use the family of cubic B-spline<sup>4</sup> deformations

$$\mathcal{G} = \left\{ g(x, y) = \sum_{k=1}^K \sum_{m=1}^M w_{km} \beta_3(x/h - k) \beta_3(y/h - m) \right\}.$$

<sup>4</sup>Cubic B-spline is a function

$$\beta_3(x) = \begin{cases} 2/3 - (1 - |x|/2)x^2, & 0 < |x| \leq 1, \\ (2 - |x|)^3/6, & 1 < |x| < 2, \\ 0, & |x| \geq 2. \end{cases}$$

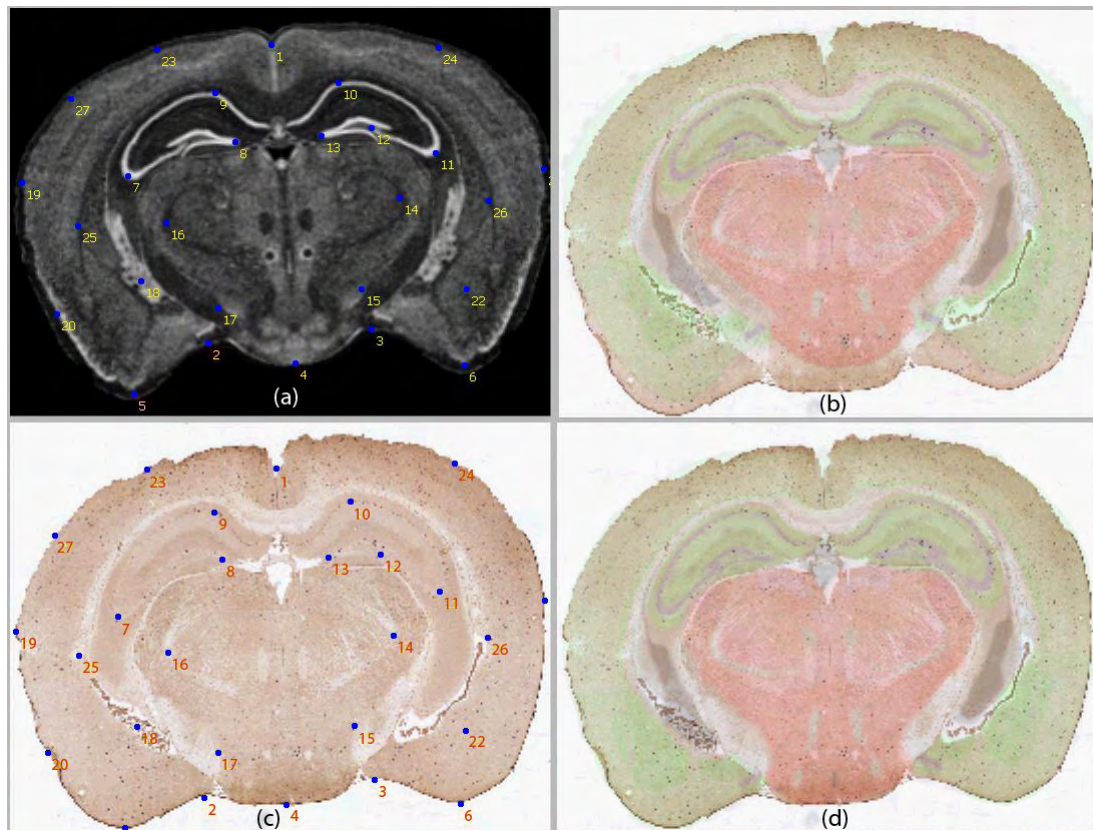


Figure 4: Example of anatomical segmentation of an ISH experimental slice. (c) – an ISH experimental slice, (a) – the corresponding to (c) virtual slice, (b) – a result of segmentation by direct transfer of anatomical map from the virtual slice, (d) – a result of segmentation with non-linear transform of the virtual slice using keypoints.

After the deformation is found it is applied to the anatomical segmentation of the virtual slice and the deformed segmentation is treated as an anatomical segmentation of experimental slice. An example of such segmentation is shown in figure 4.

### 3 Expression Detection and Image Resolution Reduction

The detection of expressing cells on ISH slices and the reduction of expression map resolution consists of the following steps:

- image preprocessing;
- extraction of the high-resolution expression map:
  - evaluating the measures of expression presence or absence;
  - combining of expression presence or absence measures into one integral characteristic to create a high resolution expression map;
- reducing expression map resolution.

There is also an additional (optional) step that includes automated quality control of the resulting map and the evaluation of integral characteristics of the resulting expression map.

#### 3.1 Image preprocessing

Image preprocessing is an optional step that is performed in a fully automated or semi-automated mode. Formally, this step can be omitted, but in this case manual tun-

ing of parameters may be required in order to achieve good quality of expression map extraction.

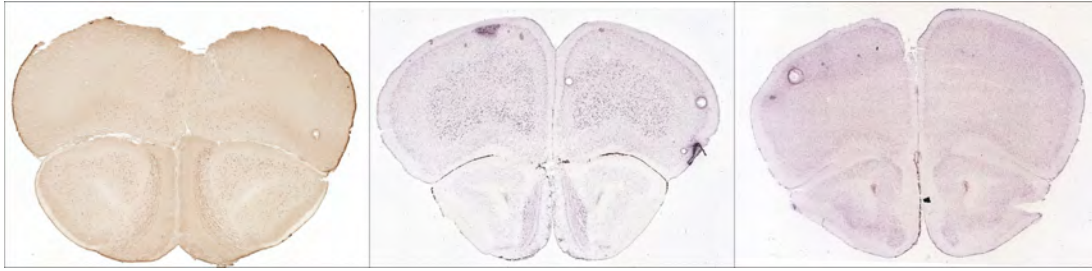


Figure 5: Examples of slice images. Left: an image from experiments carried out in Anokhin Institute of Normal Physiology (The Russian Academy of Medical Sciences); middle and right: images from Allen Mouse Brain Atlas [6, 7].

The main goal of image preprocessing is color and intensity normalization. Due to technical reasons (different illuminance conditions, non-identical coloring agents, etc.) slice images may differ (see Fig. 5), and hence different thresholds and other parameters are required in order to find expression map of good quality for different slice images. Individual estimation of parameters can be replaced by preprocessing that unifies global characteristics of an image.

The preprocessing is based on the analysis of color intensity histograms. At first we construct the grey-scale intensity histogram, separate out the background and recolor it into the fixed color (e.g. white) and in fact exclude it from the further analysis. Then, we perform the intensity/color normalization using affine transformation applied to the intensities of red, green and blue color components  $(r, g, b)$ . The transformation  $A_{opt}$  that minimizes the difference between smoothed color histograms with the predefined “standard” ones is used.

The deviation of the transformation  $A_{opt}$  from the identity transformation (in other words, the deviation of transformation matrix from the identity matrix and shift vector from zero one) can be treated as an indirect image quality control characteristic that shows the difference between “standard” experiment conditions (such as illuminance, color-agent properties, etc.) and the conditions of the studied experiment. This deviation can be measured with the discrete analogue of the following formula:

$$\int_0^1 \int_0^1 \int_0^1 \| (r, g, b) - A_{opt}^{-1}(r, g, b) \|_w p(r, g, b) dr dg db,$$

where  $p(r, g, b)$  is the probability density of observed color  $(r, g, b)$  in “standard” slice images and  $\| \cdot \|_w$  is a weighted  $l_1$ -norm with weights  $w = (w_r, w_g, w_b)$  (all color intensities are assumed to be in  $[0; 1]$ ).

### 3.2 Extraction of the high-resolution expression map

The high-resolution expression map is an image of the same size as the initial image whose pixels show the probabilistic measure of the fact that the corresponding pixel in the initial image is located in the expressing nucleus. Instead of using discrete categories (expression presence / expression absence, or high / moderate / low / no expression), we use continuous (probabilistic) expression measure. In particular, it allows to deal with intermediate categories in a more correct way and hence to achieve better quality after resolution reduction.

To obtain the final expression measure we combine several rough measures. Two types of rough measures are used: “pointwise measures” and “neighborhood measures”.

Pointwise measures evaluate the level of expression presence or absence based on the color intensities of the studied pixel only. In order to reduce computational expenses (such reduction is important due to very high image resolution) we use the point-wise measure:  $\sigma(c \cdot r) = \sigma(w_r r + w_g g + w_b b)$ , where  $c = (r, g, b)$  stands for the color of the pixel,  $w = (w_r, w_g, w_b)$  are some coefficients, and  $\sigma$  is a sigmoid-type function. A sigmoid-type function is a non-decreasing continuous function which equals zero if the argument is less than a threshold and equals one if the argument is greater than another threshold. In the simplest case it is a piecewise-linear (first degree spline) function:

$$\sigma(x) = \begin{cases} 0, & x \leq T_{min}, \\ \frac{x - T_{min}}{T_{max} - T_{min}}, & x \in (T_{min}, T_{max}), \\ 1, & x \geq T_{max}. \end{cases}$$

In this paper we use more smooth sigmoid-type functions that are second and third degree splines.

The usage of several pointwise measures is explained by the fact that the projections of regions in the three-dimensional color cube corresponding to color intensities typical for the expression presence and absence on a one-dimensional subspace are partially mixed. Projecting the data to several one-dimensional subspaces helps to reduce the number of cases when expression presence or absence is unclear. In [3], e.g., two projections (or, equivalently, two pointwise measures) are used: the first one allows to determine the pixels where the expression presence is clear, and the second one — the pixels where the expression absence is clear.

Neighborhood measures are also based on the one-dimensional (grey-scale) color  $(w_r r + w_g g + w_b b)$  instead of the three-dimensional color intensities  $(r, g, b)$ . Neighborhood measures are evaluated based on the neighborhood of the analyzed point: the sigmoid-type functions are applied either to the difference between the color of the analyzed pixel and the mean color of the neighborhood, or to the mean color of the neighborhood (it allows to detect and shadow certain types of the artifacts).

After individual measures are evaluated, they are combined into the resulting measure in the following way:

$$P = \exp(\alpha_1 \ln P_1 + \alpha_2 \ln P_2 + \dots + \alpha_N \ln P_N) = P_1^{\alpha_1} \cdot P_2^{\alpha_2} \cdot \dots \cdot P_N^{\alpha_N},$$

where  $N$  is the number of individual measures,  $P_1, P_2, \dots, P_N$  are the values of individual measures, and  $\alpha_1, \alpha_2, \dots, \alpha_N$  are the weights ( $\alpha_j \geq 0$ ). By default, all weights  $\alpha_j$  are equal to  $1/N$ , and the resulting measure is the geometrical mean. Such averaging is more efficient in comparison to the (weighted) arithmetical mean due to the probabilistic nature of measures. If required, in the semi-automated mode user can adjust the weights of individual measures. For example, user may turn off the measure that mainly shadows the artifacts in case of high-quality images with no artifacts, and, on the contrary, increase the weight of this measure in case of poor-quality images. Note that adjustment of weights can be replaced by changing sigmoid-type functions used for the evaluation of individual measures as a positive power of a sigmoid-type function is also a sigmoid-type function.

### 3.3 Reduction of the expression map resolution

Shortly speaking, the reduction of expression map resolution is performed by the convolution with an appropriate kernel and rescaling by sigmoid-type function. The initial (high-resolution) expression map is divided into rectangles corresponding to the pixels of low-resolution expression field, and for each rectangle  $\Delta_{j,k}$  the measure of expression is calculated as an integral of the product of the high-resolution expression

$$\text{Expr}_{\text{lowres}}(j, k) = \sigma \left( \int \int_{(x,y) \in \text{supp } K_{j,k}} \text{Expr}_{\text{highres}}(x, y) K_{j,k}(x, y) dx dy \right),$$

where  $\sigma$  is a sigmoid-type function,  $\text{supp } K_{j,k}$  is the support of the kernel  $K_{j,k}$  or, in other words, the neighborhood of the rectangle  $\Delta_{j,k}$ . We used kernel  $K_{j,k}$  given by formula  $K_{j,k}(x, y) = C(1 - \sigma(\text{dist}\{\Delta_{j,k}; (x, y)\}))$ . This measure equals a constant  $C$  inside the rectangle  $\Delta_{j,k}$ , equals zero outside the neighborhood of this rectangle, and continuously goes to zero in the middle zone.

Note that in the low-resolution expression field the value in each pixel is not the probabilistic measure of expression presence or absence, but a characteristic of total expression in the corresponding region. For a certain kernel and sigmoid-type function this characteristic is a total area of expressing nuclei in the region. Under certain assumptions on the cells comprising the region this characteristic can be easily converted to the approximate number of expressing nuclei of this region.

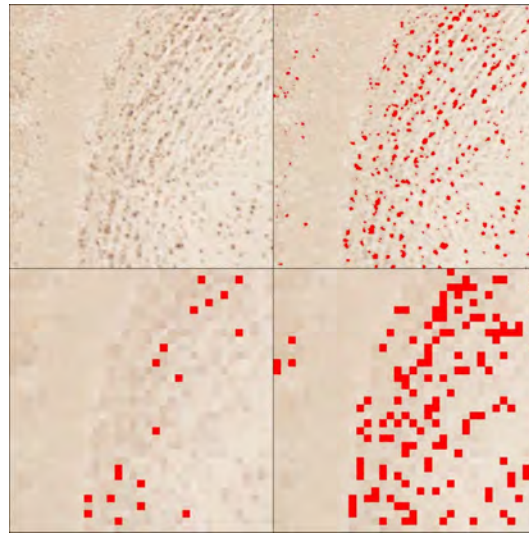


Figure 6: Examples of expression map resolution reduction. Upper-left: a fragment of a high-resolution ISH slice image; upper-right: the result of expression map extraction; lower-left: the results of expression field extraction from the low-resolution slice image; lower-right: low-resolution expression field.

The results of the reduction of the expression map resolution are illustrated in Fig. 6.

### 3.4 Postprocessing using anatomical segmentation

In case if anatomical segmentation is available, this segmentation can be used for postprocessing that includes the evaluation of integral characteristics, automated quality control and the correction of expression fields.

The main integral characteristics that can be evaluated at this step are the total expression characteristics of regions corresponding to individual anatomical structures and substructures. If images of similar slices are available for several representatives of different groups (e.g., “experiment” and “control” groups), these values can be used for rough statistical analysis that determines anatomical structures in which the activity (expression) differs significantly for different groups.

The automated quality control is based on the analysis of connectivity components of high-resolution expression map. For certain anatomical structures these components satisfy certain limitations on size and shape, but these limitations are different for different structures. For example, in many structures expressing nuclei are comparatively small and always separated by non-expressing (non-nucleic) zones, but this property



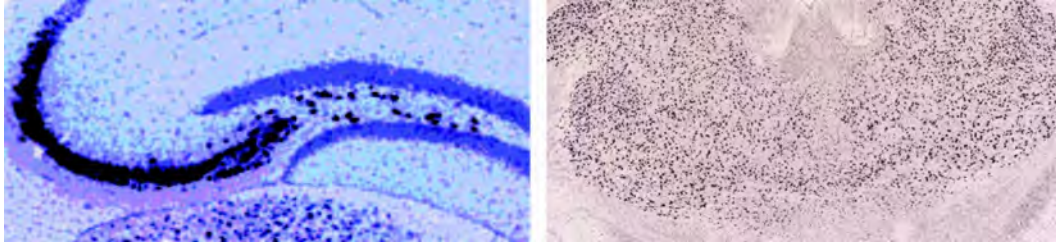


Figure 7: Example of different properties of expression fields for different structures. Left: ISH image of hippocampal region (source: [8]) — individual expressing nuclei are not separated; right: thalamus region (source: Allen Mouse Brain Atlas [6, 7]) — expressing nuclei are separated.

is violated for several structures including hippocampus and olfactory bulb [8] (see Fig. 7). If the anatomical segmentation is available, the compliance of the properties of high-resolution expression map connectivity components with theoretical limitations that hold for the corresponding anatomical structure can be tested. The quality control module reports cases of violations of the limitations and optionally shadows the corresponding connectivity component in the expression map because generally violations are explained by incorrect expression extraction caused by image artifacts.

#### 4 Discussion

We have presented algorithms for anatomical segmentation of Nissl/ISH experimental brain slices and for estimation of gene expression level on them. The solution of the first problem involved the exploitation of the 3D-model of mouse brain which we had built earlier [5] based on Allen mouse brain atlas. The BrainTravel software which we developed allows us to register an experimental slice within the model by finding the most similar virtual slice, and to deform the anatomical structures on the virtual slice from the model so that it matches the experimental slice. Thus we obtain a valid anatomical segmentation of the experimental slice. Note that despite the alternative methods based on the use of Markov Random Fields [2] this method is not limited by the number of anatomical structures it may discover. The estimation of expression level is performed in a separate procedure and the results can be loaded into the BrainTravel. Finally we can unite the results of segmentation with the expression level (see fig. 4d). This union opens vast perspectives for further cognitive research since it becomes possible to include the knowledge about anatomical structures in the statistical analysis of gene expression. Potentially this should lead to more elaborate bioexperimental design and the discovery of new genes and anatomical zones which are activated during cognitive activity of an animal.

#### Acknowledgments

The work was supported by the Russian Foundation for Basic Research (projects Nos. 09-04-12215, 08-01-00405).

#### References

- [1] J. Bolyne, E.F. Lee, A.W. Toga. "Digital Atlases as a Framework for Data Sharing". *Frontiers in Neuroscience*, vol. 2, pp. 100–106, 2008.
- [2] M. Bae, R. Pan, T. Wu and A. Badae. "Automated Segmentation of Mouse Brain Images Using Extended MRF". *NeuroImage*, vol. 46, issue 3, pp. 717–725, 2009.
- [3] J. Carson, T. Ju, C. Thaller, J. Warren, M. Bello, I.A. Kakadiaris, W. Chiu and G. Eichelle. "Automated characterization of gene expression patterns with an atlas of the mouse brain". *Proc. 26th Annual Int. Conf. of the IEEE Engineering in Medicine and Biology Society*, vol.2, pp. 2917–2920, 2004.
- [4] G. Hermosillo, C. Chefhotel and O. Faugeras. "Variational methods for multimodal image matching". *Int. J. Comput. Vis.*, vol. 50, pp. 329–343, 2002.

- [5] A. Osokin, D. Vetrov, D. Kropotov. "3-D Mouse Brain Model Reconstruction from a Sequence of 2-D Slices in Application to Allen Brain Atlas". *F. Masulli, L. Peterson, and R. Tagliaferri (Eds.): CIBB 2009, LNBI 6160*, pp. 291-303, 2010.
- [6] E.S. Lein et al. "Genome-wide atlas of gene expression in the adult mouse brain". *Nature*, vol. 445, pp. 168–176, 2007.
- [7] Allen Mouse Brain Atlas [Internet]. Seattle (WA): Allen Institute for Brain Science. © 2009. Available from: <http://mouse.brain-map.org>.
- [8] L. Ng, S.D. Pathak, M. Hawrykycz et al. "Neuroinformatics for Genome-Wide 3D Gene Expression Mapping in the Mouse Brain". *IEEE/ACM Transactions on Computational Biology and Bioinformatics*, vol. 4, no. 3, pp. 382–393, 2007.
- [9] T. Ju, J. Warren, J. Carson et al. "3D volume reconstruction of a mouse brain from histological sections using warp filtering". *Journal of Neuroscience Methods*. vol. 156, no. 1-2, pp. 84–100, 2006.